2018 IEEE-RAS 18th International Conference on Humanoid Robots (Humanoids)
Beijing, China, November 6-9, 2018

The eLeg: A Novel Efficient Leg Prototype Powered by Adjustable Parallel Compliant Actuation Principles

Zeyu Ren, Wesley Roozing, and Nikos G. Tsagarakis

Abstract— **This paper presents the design and implementation details of an efficient robotic leg (eLeg) prototype in which series-elastic actuation is combined with adjustable parallel compliance to significantly improve its energy efficiency. The parallel actuation units are driven by secondary motors to adjust pretension of the parallel elasticity. Both monoarticulated and biarticulated actuation configurations can be employed and the leg was thus designed to permit rapid reconfiguration of its actuation units for the purpose of performing validation studies and energetic comparison of the different actuation configurations. We focus on the design procedure and implementation of the adjustable parallel actuation units, including elastic element selection, mechanism design, and force sensing capability. A design method for robots utilising the concept is presented and experimental data are provided, that demonstrate the effectiveness of both the actuation concepts and design procedure.**

I. Introduction

In the past few decades, great progress has been made in the field of robotic actuation. The most notable shift is the broad utilization of compliance in actuation, not only in series between actuators and their outputs, but also in parallel to the main actuation drives, in an attempt to resemble biological systems in terms of non-stiff actuation that provides energy storage and recycling, improving the energetic economy during various phases of the motion. Among the various types of compliant actuation, Series Elastic Actuation (SEA) is widely adopted, originating from the work of Pratt in the 90s [1]. Its advantages in enhancing energy efficiency [2], [3], robust torque control ability [4]–[7], and physical robustness [8], [9] have been well verified. In contrast, Parallel Elastic Actuation (PEA) is less adopted than SEA but its benefits also have been significantly demonstrated in actuator test bench setups [10]–[13], bipedal walkers [14], [15], humanoids [16], and exoskeletons [17]. Inspired by biarticulated muscle configurations in biological systems [18], some works have utilized biarticulated mechanisms to transfer mechanical power between joints [19] and improve the end-effector force ellipsoid [20].

In our previous work, we proposed a mixed series-parallel compliant actuation concept which we refer to as Asymmetric Compliant Actuation (ACA), in which a high power SEA branch is combined with an actively adjustable parallel high efficiency elastic energy storage branch. We experimentally verified the potential of this concept on a 1-DoF leg prototype [21], resulting in a 65% reduction in electrical power consumption compared to conventional SEA only [22]. Based on that work, in [23] the concept was generalised to multi-DoF articulated robots and biarticulated configurations, and a simulation study demonstrated significant advantages in further improving energy efficiency and reduction in peak torque. Motivated by these promising results, a novel 3-DoF leg prototype (eLeg) based on this concept was developed [24] (Fig. 1), both with monoarticulated and biarticulated parallel elastic actuation configurations. Initial experimental results demonstrated significant energy efficiency improvements of 53% and 60% in electrical power consumption compared to SEA only, combined with significantly reduced RMS and peak torque requirements on the main SEA actuators.

The authors are with Humanoids and Human Centered Mechatronics Lab (HHCM), Istituto Italiano di Tecnologia (IIT), Via Morego 30, 16163 Genova, Italy. E-mail: {zeyu.ren, wesley.roozing, nikos.tsagarakis}@iit.it

Fig. 1: Squatting eLeg in monoarticulated configuration with 20 kg load. In contrast, the robot weighs only 10.9 kg.

This work focuses on the detailed mechanical design of the efficient leg (eLeg) prototype, specifically realization of the vital adjustable parallel elastic actuation unit, denoted as Energy Storage Branch (ESB). We present the design procedure and implementation, including elastic element selection, mechanism design, and force sensing capability. Experimental data demonstrates the design's effectiveness.

This paper is structured as follows. Sec. II briefly introduces the actuation concept, followed by an overview of the eLeg design in Sec. III. Sec. IV presents the design procedure and implementation of the ESB unit. Experimental validation is presented in Sec. V, and lastly, conclusions and suggestions for future work are discussed in Sec. VI.

II. Actuation Concept

The actuation concept utilized on the eLeg robot is Asymmetric Compliant Actuation (ACA) [21]–[24] as shown in Fig. 2. It consists of two parallel compliant actuation

978-1-5386-7282-2/18/$31.00 ©2018 IEEE

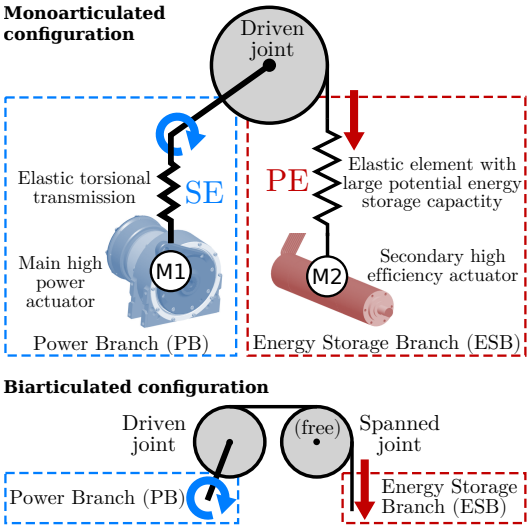

Fig. 2: The series-parallel actuation concept we refer to as Asymmetric Compliant Actuation (ACA), shown in both monoarticulated and biarticulated configuration.

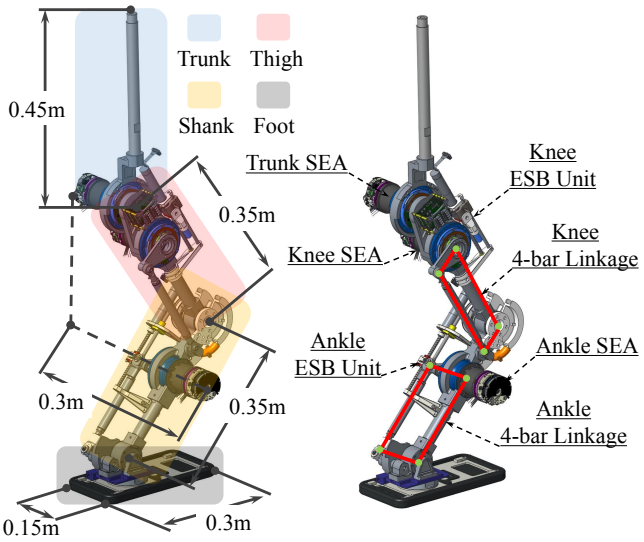

Fig. 3: The eLeg prototype in monoarticulated configuration, showing overall dimensions and major components.

branches. The first branch, denoted the Power Branch (PB), is a rotary series-elastic actuator with elastic element SE, and the second branch, referred to as the Energy Storage Branch (ESB), comprises a highly-efficient lower power motor with high reduction linear transmission. In the monoarticulated configuration shown on the top of Fig. 2, the ESB motor M2 is coupled to the driven joint through a linear unidirectional series elastic element PE and pulley. The elastic element PE differs from SE in its significantly lower stiffness and much larger energy storage capacity.

Shown on the bottom of Fig. 2 is the ACA concept in biarticulated configuration, in which the ESB tendon spans a free pulley on a second (so-called spanned) joint, before driving the first. Compared to the monoarticulated configuration, here the elongation of elastic element PE is a function of the configuration of both joints, and it provides torque to both joints. Selection of the pulley radii and stiffness value allows to shape the torque profile as a function of both joint configurations and pretension position of the motor M2. This property of biarticulation is useful as 1) in general the loading on a joint depends on the configuration of multiple joints, and 2) it allows for mechanical power transfer between joints, as is also observed in humans [18].

III. 3-DoF Leg Design - eLeg

The design of the eLeg prototype is inspired by the human biological counterpart [25] and existing humanoid robot designs. Based on their parameters, target specifications for dimensions and weight were set. The design features three actuated degrees of freedom: ankle, knee and hip. We opted for a leg size slightly under average human size, and aimed for mass not exceeding the human limb and with similar mass distribution; resulting in a semi-anthropomorphic design corresponding to a $\approx 1.50\,\text{m}$ humanoid.

The dimensions and major components for the prototype in monoarticulated configuration are shown in Fig. 3, and corresponding design parameters and mass distribution are summarized in Table I. The total mass for the SEA-only, monoarticulated and biarticulated actuation configurations are 9.3 kg, 10.9 kg, and 10.9 kg, respectively, with the mass of both leg segments (thigh and shank) smaller than that of the human limb in the biarticulated case (Table I). To minimise the leg's inertia with respect to the hip joint, the ankle and knee actuators are placed high on the leg segments, and drive the joints through parallelogram four-bar linkages. The utilized actuators are three identical medium-sized SEAs [26], for which details are also shown in Table I.

The required range of motion of the robot's joints is highly dependent on the desired motions. To be precise, two configurations, namely a deep squat posture requiring high ankle and knee flexion [27], [28], and jumping posture in which the ankle is highly extended [28], need to be realized. Hence, the knee joint is designed to achieve a range of motion of $[0°, 130°]$, and the ankle joint is designed to reach a bi-directional working range of $[-69°, 54°]$, which satisfy these requirements. The trunk joint is capable of rotating in a large range of $[-150°, 150°]$ to allow balancing the trunk in any leg posture, and control the center of pressure.

The leg was designed to permit the implementation of three distinct actuation configurations [24], to show both the potential of our proposed actuation concept as well as investigate the effectiveness of biarticulated actuation configurations:

- **SEA only**: Actuated exclusively by SEAs, to serve as a baseline actuation arrangement which is common in most state-of-the-art articulated robot designs;
- **Monoarticulated**: Ankle and knee joints are each augmented with a monoarticulated ESB (Fig. 1,3,4);
- **Biarticulated**: Again featuring two joints with ESBs, however in this case one of the ESBs is biarticulated: The tendon for the ankle spans the knee joint and is driven by a motor on the back of the thigh (Fig. 4).

TABLE I: The eLeg design and actuation parameters for each actuation configuration.

Leg Dimensions and Mass Distribution				
	Trunk[(1)]	Thigh	Shank	Foot
Dimensions	0.45 m	0.35 m	0.35 m	$0.28 \times 0.15 \times 0.06$ m
Mass: SEA	1.86 kg, 20.0%	2.79 kg, 30.0%	2.95 kg, 31.7%	1.70 kg, 18.3%
Mass: Monoarticulated	1.86 kg, 17.0%	3.58 kg, 32.8%	3.78 kg, 34.6%	1.70 kg, 15.6%
Mass: Biarticulated	1.86 kg, 17.1%	4.22 kg, 38.9%	3.07 kg, 28.3%	1.70 kg, 15.7%
Mass: Human limb [25]:	n.a.	7.88 kg	3.38 kg	1.13 kg

Joint Actuation SEAs [26], [29] Configuration				
Motor Type	Gearbox Type	Gear Ratio	Stiffness	Peak Torque
Kollmorgen TBMS-6025	Harmonic Drive CPL-20	80 : 1	5800 Nm/rad	127 Nm
Torque Sensing		Position Sensing		
Angle deflection based, 69 mNm resolution		Renishaw AksIM 19 bit absolute position encoder		

Joint Working Range[(2)]		
Trunk Joint: $[-150°, 150°]$	Knee Joint: $[0°, 130°]$	Ankle Joint: $[-69°, 54°]$

Note: (1) The trunk mass does not include the 20 kg weight mounted on it to simulate the weight of a full humanoid robot; (2) The counter-clockwise rotation direction in Fig. 3 is defined as positive joint rotation.

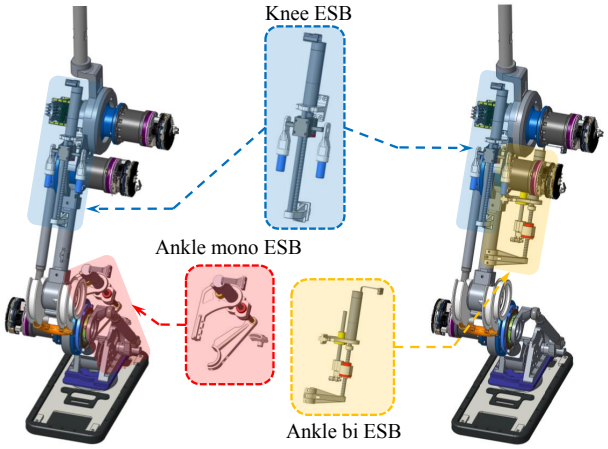

Fig. 4: Reconfigurable actuation arrangements: Monoarticulated (left) and biarticulated (right) configurations.

As a result, the leg and ESB units are designed such that switching between actuation configurations can done rapidly and conveniently. Fig. 4 shows the placement of ESB units for the mono- and biarticulated configurations (SEA only configuration not shown as it has no ESBs). The elastic elements are not shown. Each ESB unit requires only two connectors and roughly eight screws to mount. In the following Section we elaborate on the detailed design procedure for the ESB units and selection of their parameters.

IV. ESB Units - Design & Implementation

A. Requirements & Design Concepts

The main novelty of the actuation concept is the inclusion of the Energy Storage Branch with its compliant energy storage. For their design, the main requirements are as follows (where we provide approximate target values for the knee unit, which is the most demanding joint):

- Large maximum storage capacity (order of 100 J);
- Sufficient torque capacity (up to approx. 100 Nm);
- High torque/weight and energy storage/weight ratio;
- Rapid reconfiguration (ESB units must be mountable and dismountable within 5 minutes).

Several implementations were considered to achieve the desired properties, including metal and pneumatic springs, where the latter was quickly discarded due to higher difficulty for reliable implementation and the need of a secondary (pneumatic) power unit.

Three options were considered in more detail: rubber-type elastic cords enclosed in nylon sheaths [21], [22], linear metal extension springs [16], [30], and metal torsion springs [31]. However, due to the requirements of biarticulated configurations and size and weight requirements, as well as integration complexity, torsional springs turned out to be unsuitable. Linear metal springs appear to be a viable option, however in terms of energy storage capacity to weight ratio they are vastly outperformed by rubber-type elastic materials. Hence, as in the previous prototype [22], the final design is based on rubber-type elastic cords, which we shall refer to as "bungees" for simplicity.

B. Bungee Selection

The design optimisation procedure [23] used to select elastic element stiffness, pulley radii and default pretension position of the ESB units assumes a linear stiffness profile of the elastic elements, with zero rest length. However, the rubber-type materials used typically have an S-shaped elongation–force curve, in which force increases rapidly for the first 10-20% (of rest length) of elongation, then flattens out, to increase rapidly again at roughly 80%. Two parameters are dominant in selecting a cord to approximate a desired linear stiffness: the rest length l_r and diameter d. Considering the nonlinearity of the stiffness profile, we determine the linear stiffness k_l of the bungee by linearisation of the aforementioned S-shaped curve from datasheets at 35% elongation, resulting in a good overall fit. The linear stiffness is then given by

$$k_l = \frac{f_p(d)}{0.35\, l_r}, \tag{1}$$

where f_p is the extension force at 35% elongation and is dependent on the bungee diameter d.

Besides the desired linear stiffness, there are two length requirements. Firstly, the element should fit within the avail-

TABLE II: ESB unit bungee parameter selection, for both the monoarticulated (*mono*) and biarticulated (*bi*) configurations. Optimal stiffness and required elongation follow from the design parameter optimisation procedure [23] followed by extensive simulation.

Bungee Parameters and Computed Parameters								
Bungee	Req. Elongation l_e [cm]	Opt. Stiffness k_d [kN/m]	Min. Length l_m [cm]	Avail. Length l_a [cm]	Chosen Rest Length l_r [cm]	Chosen Diameter d [mm]	Stiffness, err. k_l [kN/m]	
Ankle (mono)	7.7	5.4	9.6	12.0	12.0	12	5.8, 8.0%	
Ankle (bi)	1.9	29.2	2.4	43.3	6.5	18	29.0, -0.6%	
Knee (mono)	25.0	8.3	31.3	48.0	45.5	13	7.8, -6.2%	
Knee (bi)	29.0	8.3	36.3	48.0	45.5	13	7.8, -6.2%	
Bungee Extension Force f_p (at 35% Elongation)								
Diameter [mm]	10	11	12	13	14	15	18	20
Force [N]	140	180	245	310	420	530	660	790

able space l_a along the leg segment. Secondly, the amount of elongation required should not exceed the allowed elongation of the material, chosen to be 80%. These requirements are summarised as:

$$l_m \leq l_r \leq l_a, \quad \text{where} \quad l_m = \frac{l_e}{0.8}, \tag{2}$$

the value of l_e is derived from extensive simulation of the prototype, and l_m denotes the minimum bungee rest length. Table II lists the previously mentioned ESB elastic element parameters for all three actuation configurations, which result from the design parameter optimisation procedure from [23] followed by extensive simulation. Following selection of rest lengths and diameters, the achieved (linearised) stiffness, their desired values, and error margins are given in Table II, which are within 8%. Finally, the last rows of Table II list the bungee cord properties as provided by the manufacturer.

C. Actuation Mechanism Design

The elastic elements must be linearly driven to adjust their pretension. A rotational motor with gearbox combined with a ball screw transmission mechanism are chosen to provide pretension regulation, due to their compact integration, small weight, and large linear motion range. In the following design procedure, we provide numerical examples for the knee joint ESB, as it is the highest loaded joint in the leg.

Starting with the ball screw, the pitch p is a crucial parameter that is selected as a trade-off between dynamic loading capacity and additional gearbox ratio required to amplify the motor torque prior to the ball screw transmission. The ball screw's permitted dynamic load f_d should be chosen larger than the maximum experienced dynamic force f_d^{max} according to the maximum bungee extension force in Table II, written as:

$$f_d \geq f_d^{max}\, S = \frac{l_e}{2}\, k_l\, S, \tag{3}$$

where the values for l_e and k_l are those of the most demanding biarticulated configuration, and the safety factor S is set as 1.5. l_e is divided by two due to the fact the bungee is wrapped around at the knee and the other side attaches to the other side of the ball screw nut forming a dual bungee elastic element. The resulting minimum dynamic load is obtained as $f_d \geq 1700\,\text{N}$. Conversely, the generated linear force f_l transmitted through the ball screw and gearbox should not exceed the motor's continuous torque capability,

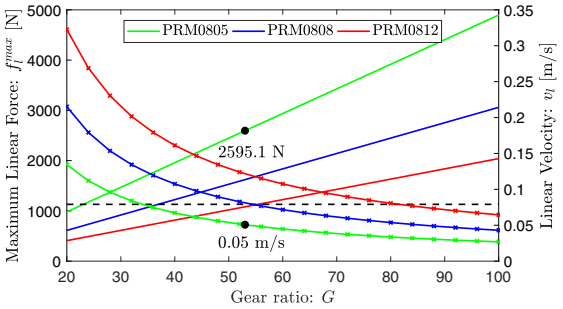

Fig. 5: Maximum linear generated force f_l^{max} (solid lines) and linear velocity v_l (curves with crosses) for three ball screw types as a function of gearbox transmission ratio G.

which favours larger total gear ratios. In fact, increasing the transmission ratio reduces the loading on the motor, improving energy efficiency at the cost of reduced adjustment velocity. The maximum continuously generated linear force f_l^{max} and linear velocity v_l are computed as

$$f_l^{max} = I_{max}\, k_\tau\, \eta_m\, \frac{2\pi\, G}{p}, \tag{4}$$

$$v_l = V_n\, k_\tau^{-1}\, \frac{p}{2\pi\, G}, \tag{5}$$

where k_τ denotes the torque constant of the motor, I_{max} and V_n denote the maximum continuous current and operating voltage of the motor, G denotes the gearbox transmission ratio, and η_m denotes the combined gearbox and ball screw efficiency, set as 0.8 by considering the low operating speeds at high loading.

Given the goals of light weight and compact integration of the mechanism, the Thomson Miniature Series ball screw was selected. Candidate models are listed in Table III. As can be observed, dynamic loading capacity increases with increased pitch p. Hence, to satisfy the dynamic load requirement (3), we focus on the models PRM0805, PRM0808, and PRM0812. As the ESB speed requirements are small due to a limited required working range, and to avoid necessitating the use of a large and heavy motor, a lightweight combination of Maxon EC 22 brushless motor and Maxon GP 22 HP planetary gearbox was chosen, giving high efficiency and compactness, as shown in Table III.

The resulting maximum generated linear force f_l^{max} and linear velocity v_l are shown in Fig. 5 as a function of gearbox ratio G for each of the three ball screw models. From the

TABLE III: ESB unit drive train mechanism parameters.

Thomson Miniature Ball Screw Series selection[1]								
Type	PRM0401	PRM0504	PRM0601	PRM0606	PRM0801	PRM0805[2]	PRM0808	PRM0812
Diameter d_b, Pitch p [mm]	4 , 1	5 , 4	6 , 1	6 , 6	8 , 1	8 , 5	8 , 8	8 , 12
Max. dynamic Load f_d [N]	790	720	1200	1450	780	1850	3800	4000
Motor: Maxon EC 22 Brushless 386675[3]								
Torque Constant k_τ [mNm/A]			Maximum Continuous Current I_{max} [A]			Nominal Voltage V_n [V]		
14.2			3.43			48		
Gearhead: Maxon Planetary GP 22 HP								
Knee ESB: 53:1 (Mono & bi)						Ankle ESB: 29:1 (Mono & bi)		

Note: (1) Considering compact and lightweight design, ball screws up to 8 mm diameter were considered; (2) Finally chosen model; (3) For standardization, the same type of motor is selected for all ESB units.

force requirement derived from the required elongation and stiffness, the maximum generated force f_l^{max} is ≈ 1130 N, shown by the dashed line in Fig. 5. While all three ball screws can satisfy this requirement at different gearbox ratios, consider that increased pitch requires a larger gear ratio G which further reduces the overall drivetrain's efficiency. Hence, the final choice of ball screw and gearbox is obtained as small pitch p and small gear ratio G.

Based on this analysis, we finally selected the PRM0805 ball screw with 5 mm pitch and gear ratio $G = 53$ for the knee ESB, indicated by the black dots in Fig. 5. With this choice, the maximum linear force is 2595.1 N and linear velocity is 0.05 m/s, which allows to traverse the entire pretension working range in 2.5 seconds, which is sufficient for the parallel branches as fast adjustment is less efficient and not required for accurate joint torque control due to the main series-elastic drives. For the ankle ESB, loading is much smaller than the knee ESB under both mono- and biarticulated configuration. Thus, the same ball screw type and gearbox with lower gear ratio were selected as shown in Table III, allowing for some interchange of components as well if needed.

D. Modifications for High Loading Conditions

To maximise structure compactness, all ESBs were originally designed to be single-sided, that is, a single elastic element was used which was pretensioned by the ball screw, as shown in the left-hand side of Fig. 6. However, due to very high loading on the knee joint, this led to failure of several ball screws while adjusting pretension under load, due to excessive torsional moments on the nut. Hence, the knee unit was implemented using a single, longer element, both ends of which are attached to the ball screw nut and pass through a track on the knee (right side of Fig. 6). As the net line of force is now through the ball screw itself, this reduces the torsional moment on the nut to a minimum.

A section of the knee joint is shown in Fig. 7. It shows both main knee pulleys and the track that connects them, routing the bungee around back to the ESB unit's ball screw nut. Inside the right-hand side pulley, the free pulley can be seen that is used for the biarticulated configuration, routing the ankle bungee to its ESB unit on the back of the thigh.

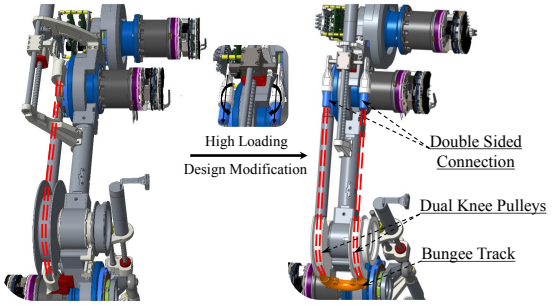

Fig. 6: Modification of the knee ESB unit to improve robustness against high loading.

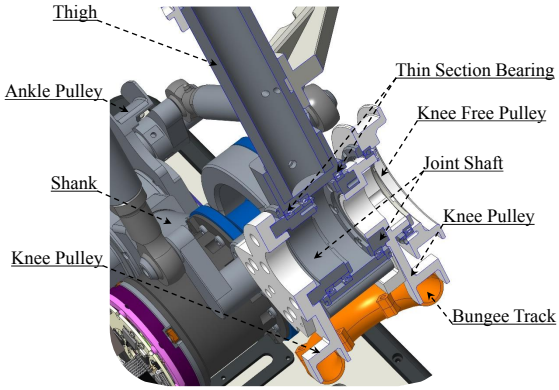

Fig. 7: Section of the knee joint.

E. Force-sensing Ball Screw Nut

The installation of the ESB units incorporate two mounting points and a single linear guide to avoid nut rotation (Fig. 8(a)). Each unit was augmented with an instrumented ball screw nut, with steel cantilever beams and strain gauges to obtain accurate measurements of the linear force applied by the bungees, as well as provide mounting points for the bungee hooks. For the knee, the beams were designed to each support 750 N of force. Fig. 8(b) shows the finite-element analysis (FEA) results, where the stress was controlled to be under the yield stress of 17-4PH steel and displacement and strain were controlled to appropriate values to ensure force measuring sensitivity. The strain gauge surfaces were designed to have nearly homogeneous strain. The design achieves excellent force sensing capability, with high linearity, as shown in Fig. 8(c).

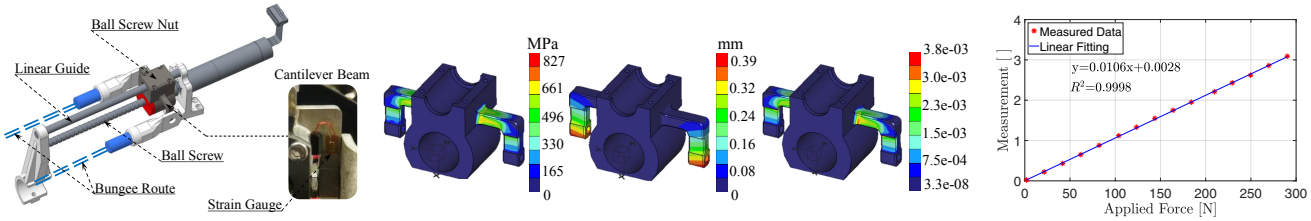

(a) Complete ESB unit for the knee joint. (b) FEA results: stress, displacement and strain. (c) Force sensing linearity.

Fig. 8: ESB unit design overview and force sensing.

V. Experimental Validation

To demonstrate the effectiveness of the actuation concepts and design procedure for the ESB units, we provide experimental data obtained during cyclic deep squatting motions, with the leg in monoarticulated actuation configuration and loaded with 20 kg weight at the trunk. Contrary to our earlier preliminary experiments [24], we focus on the knee ESB, and adjust the pretension during the motion. Furthermore, instead of position control, the entire robot was torque controlled, where the torque generated by the ESB (obtained from the linear force measurements) was subtracted from the impedance torque reference to compute desired SEA torque and achieve accurate joint-level impedance control, i.e.:

$$\tau^*_{SEA} = K\,(q^* - q) + D\,(\dot{q}^* - \dot{q}) - \tau_{ESB} \qquad (6)$$

where K, D denote the joint impedance parameters, q^* and q denote the joint equilibrium and actual position, respectively, and τ_{ESB} denotes the measured ESB torque.

Fig. 9 shows the results. Following two increases in pretension from 5 mm to 85 mm as shown in Fig. 9(a)-9(b), the RMS torque provided by the SEA is reduced from 42 Nm to 20 Nm, as the torque provided by the ESB increases (Fig. 9(c)). Meanwhile, the net knee torque remains constant to achieve the desired motion profile. For demonstration purposes a low adjustment speed of 3 mm/s was used. After the increase in pretension, the linear force applied on the ball screw mechanism from the bungee can be seen in Fig 9(d) to reach 1190 N, which verifies the robustness of the ESB unit design under high load.

Fig. 9(e) shows the SEA (PB), ESB, and net electrical power of the knee joint. Despite the same net torque (and mechanical power) being provided at the joint, the cycle mean net electrical power decreases from 29.7 W to 11.1 W as the ESB is pretensioned, a significant improvement in energy efficiency of 63%. Particularly, it can be observed that the power of the ESB unit is negligible. However, it can be observed that at 5 mm pretension the ESB is already providing nearly half of the torque requirements; if the pretensioned case would be compared to the case where the ESB was dismounted (SEA only), the difference in electrical power consumption would be significantly larger.

VI. Conclusions & Future Work

This paper has presented the design and implementation of adjustable compliant actuation units, which are based on a series-parallel compliant actuation concept called Asymmetric Compliant Actuation (ACA) and aims to significantly enhance the energy efficiency and explosiveness of articulated robots through energy storage. This concept was employed to realize an efficient leg (eLeg) prototype, which can be configured in three different actuation configurations, including a bio-inspired topology where one of the tendons is biarticulated. Based on numerical design optimisation and extensive simulations, design requirements were derived. Based on these requirements, details of the design procedure and implementation of the eLeg were discussed, including selection of the elastic elements, mechanism design, and force sensing, which allow to design such actuation units for general articulated robots. Experimental data was presented that show that the realized parallel actuation units satisfy the design requirements and significantly improve the energetic efficiency of the robot. These results demonstrate the effectiveness of the actuation concept and design methods.

In the presented experiments, the parallel actuation units were manually controlled. Implementation of an integrated control strategy that adjusts them based on the joint torque requirements is the subject of ongoing efforts, and the results of these will be presented in future works. Furthermore, a more thorough comparison between monoarticulated and biarticulated actuation configurations will be investigated. Finally, more complex and dynamic motions such as explosive motions and jumping are considered.

Acknowledgment

This work is supported by European Commission projects CENTAURO (644839) and CogIMon (644727).

References

[1] G. A. Pratt and M. M. Williamson, "Series elastic actuators," in *IEEE/RSJ International Conference on Intelligent Robots and Systems*, vol. 1, 1995.

[2] D. Paluska and H. Herr, "The effect of series elasticity on actuator power and work output: Implications for robotic and prosthetic joint design," *Robotics and Autonomous Systems*, vol. 54, no. 8, 2006.

[3] A. Velasco, G. M. Gasparri, M. Garabini, L. Malagia, P. Salaris, and A. Bicchi, "Soft-actuators in cyclic motion: Analytical optimization of stiffness and pre-load," in *IEEE-RAS International Conference on Humanoid Robots*, 2013.

[4] W. Roozing, J. Malzahn, N. Kashiri, D. G. Caldwell, and N. G. Tsagarakis, "On the stiffness selection for torque-controlled series-elastic actuators," *IEEE Robotics and Automation Letters*, vol. 2, no. 4, 2017.

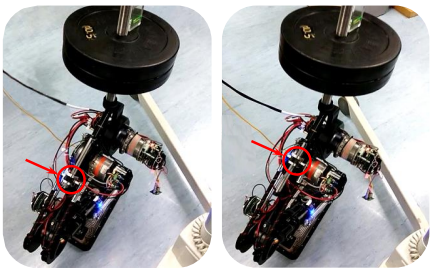

(a) 5 mm pretension (b) 85 mm pretension

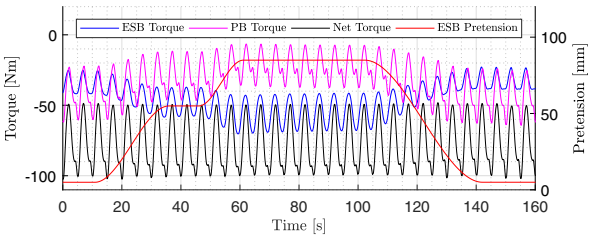

(c) Knee joint PB, ESB, and net torque.

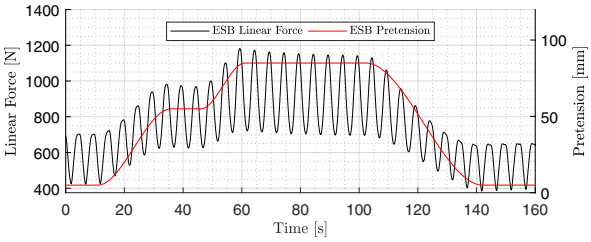

(d) Linear force as measured by the knee joint ESB unit.

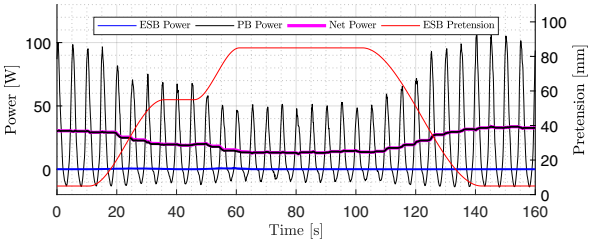

(e) PB, ESB and net electrical power of the knee joint.

Fig. 9: Experiment data: Adjusting knee ESB pretension during cyclic deep squatting motions with 20 kg trunk load.

[5] D. W. Robinson, J. E. Pratt, D. J. Paluska, and G. A. Pratt, "Series elastic actuator development for a biomimetic walking robot," in *IEEE/ASME International Conference on Advanced Intelligent Mechatronics*, 1999.

[6] A. Calanca, R. Muradore, and P. Fiorini, "A review of algorithms for compliant control of stiff and fixed-compliance robots," *IEEE/ASME Transactions on Mechatronics*, vol. 21, no. 2, 2016.

[7] H. Vallery, J. Veneman, E. Van Asseldonk, R. Ekkelenkamp, M. Buss, and H. Van Der Kooij, "Compliant actuation of rehabilitation robots," *IEEE Robotics & Automation Magazine*, vol. 15, no. 3, 2008.

[8] F. Negrello, M. Garabini, M. G. Catalano, J. Malzahn, D. G. Caldwell, A. Bicchi, and N. G. Tsagarakis, "A modular compliant actuator for emerging high performance and fall-resilient humanoids," in *IEEE-RAS International Conference on Humanoid Robots*, 2015.

[9] M. Hutter, C. Gehring, D. Jud, A. Lauber, C. D. Bellicoso, V. Tsounis, J. Hwangbo, K. Bodie, P. Fankhauser, M. Bloesch *et al.*, "Anymal-a highly mobile and dynamic quadrupedal robot," in *IEEE/RSJ International Conference on Intelligent Robots and Systems (IROS)*, 2016.

[10] U. Mettin, P. X. La Hera, L. B. Freidovich, and A. S. Shiriaev, "Parallel elastic actuators as a control tool for preplanned trajectories of underactuated mechanical systems," *The international journal of robotics research*, vol. 29, no. 9, 2010.

[11] D. F. Häufle, M. Taylor, S. Schmitt, and H. Geyer, "A clutched parallel elastic actuator concept: Towards energy efficient powered legs in prosthetics and robotics," in *IEEE International Conference on Biomedical Robotics and Biomechatronics (BioRob)*, 2012.

[12] G. Mathijssen, D. Lefeber, and B. Vanderborght, "Variable recruitment of parallel elastic elements: Series–parallel elastic actuators (spea) with dephased mutilated gears," *IEEE/ASME Transactions on Mechatronics*, vol. 20, no. 2, 2015.

[13] M. Plooij, M. Wisse, and H. Vallery, "Reducing the energy consumption of robots using the bidirectional clutched parallel elastic actuator," *IEEE Transactions on Robotics*, vol. 32, no. 6, 2016.

[14] T. Yang, E. Westervelt, J. P. Schmiedeler, and R. Bockbrader, "Design and control of a planar bipedal robot ernie with parallel knee compliance," *Autonomous robots*, vol. 25, no. 4, 2008.

[15] A. Mazumdar, S. J. Spencer, C. Hobart, J. Salton, M. Quigley, T. Wu, S. Bertrand, J. Pratt, and S. P. Buerger, "Parallel elastic elements improve energy efficiency on the steppr bipedal walking robot," *IEEE/ASME Transactions on Mechatronics*, vol. 22, no. 2, 2017.

[16] S. Shirata, A. Konno, and M. Uchiyama, "Design and evaluation of a gravity compensation mechanism for a humanoid robot," in *IEEE/RSJ International Conference on Intelligent Robots and Systems*, 2007.

[17] S. Toxiri, A. Calanca, J. Ortiz, P. Fiorini, and D. G. Caldwell, "A parallel-elastic actuator for a torque-controlled back-support exoskeleton," *IEEE Robotics and Automation Letters*, vol. 3, no. 1, 2018.

[18] G. J. V. I. Schenau, "From rotation to translation: Constraints on multi-joint movements and the unique action of bi-articular muscles," *Human Movement Science*, vol. 8, no. 4, 1989.

[19] T. J. Klein and M. A. Lewis, "A robot leg based on mammalian muscle architecture," in *IEEE International Conference on Robotics and Biomimetics*, 2009.

[20] V. Salvucci, Y. Kimura, S. Oh, T. Koseki, and Y. Hori, "Comparing approaches for actuator redundancy resolution in biarticularly-actuated robot arms," *IEEE/ASME Transactions on Mechatronics*, 2014.

[21] N. G. Tsagarakis, H. Dallali, F. Negrello, W. Roozing, G. A. Medrano-Cerda, and D. G. Caldwell, "Compliant antagonistic joint tuning for gravitational load cancellation and improved efficient mobility," in *IEEE-RAS International Conference on Humanoid Robots*, 2014.

[22] W. Roozing, Z. Li, G. A. Medrano-Cerda, D. G. Caldwell, and N. G. Tsagarakis, "Development and control of a compliant asymmetric antagonistic actuator for energy efficient mobility," *IEEE/ASME Transactions on Mechatronics*, vol. 21, no. 2, 2016.

[23] W. Roozing, Z. Li, D. G. Caldwell, and N. G. Tsagarakis, "Design optimisation and control of compliant actuation arrangements in articulated robots for improved energy efficiency," *IEEE Robotics and Automation Letters*, vol. 1, no. 2, 2016.

[24] W. Roozing, Z. Ren, and N. G. Tsagarakis, "Design of a novel 3-dof leg with series and parallel compliant actuation for energy efficient articulated robots," in *IEEE International Conference on Robotics and Automation*, 2018.

[25] A. Tözeren, *Human body dynamics: classical mechanics and human movement*. Springer Science & Business Media, 1999.

[26] L. Baccelliere, N. Kashiri, L. Muratore, A. Laurenzi, M. Kamedula, A. Margan, S. Cordasco, J. Malzahn, and N. G. Tsagarakis, "Development of a human size and strength compliant bi-manual platform for realistic heavy manipulation tasks," in *IEEE/RSJ International Conference on Intelligent Robots and Systems*, 2017.

[27] N. Dahlkvist, P. Mayo, and B. Seedhom, "Forces during squatting and rising from a deep squat," *Engineering in medicine*, vol. 11, no. 2, 1982.

[28] M. F. Bobbert, K. G. Gerritsen, M. C. Litjens, and A. J. Van Soest, "Why is countermovement jump height greater than squat jump height ?" *Medicine and science in sports and exercise*, vol. 28, 1996.

[29] N. Kashiri, J. Malzahn, and N. G. Tsagarakis, "On the sensor design of torque controlled actuators: A comparison study of strain gauge and encoder-based principles." *IEEE Robotics and Automation Letters*, vol. 2, no. 2, pp. 1186–1194, 2017.

[30] B. Vanderborght, N. G. Tsagarakis, C. Semini, R. Van Ham, and D. G. Caldwell, "Maccepa 2.0: Adjustable compliant actuator with stiffening characteristic for energy efficient hopping," in *IEEE International Conference on Robotics and Automation*, 2009.

[31] A. Jafari, N. G. Tsagarakis, and D. G. Caldwell, "Awas-ii: A new actuator with adjustable stiffness based on the novel principle of adaptable pivot point and variable lever ratio," in *IEEE International Conference on Robotics and Automation*, 2011.